Kinetics and Isotherms Study of Methylene Blue Dye Adsorption on Water Hyacinth Stem Powder Adsorbent

Anodar Ratchawet[1*], Atinut Joradol[2], Jutamas Sookyang[3], Chadaphon Bueruean[1] and Supasajee Doungjit[1]

[1]Chemistry Department, Faculty of Science and Technology, Chiangmai Rajabhat University, Chiangmai, 53000, Thailand
[2]Biology Department, Faculty of Science and Technology, Chiangmai Rajabhat University, Chiangmai, 53000, Thailand
[3]Mathematics and Statistics Department, Faculty of Science and Technology, Chiangmai Rajabhat University, Chiangmai, 53000, Thailand

∗Corresponding Email: anodar_rat@g.cmru.ac.th

Received August 24, 2024, Revised August 25, 2025, Accepted September 10, 2025, Published December 30, 2025

Abstract. *This study aims to evaluate the adsorption efficiency of water hyacinth stem powder (WHSP) to remove methylene blue (MB) dye from aqueous solutions. Batch adsorption experiments were conducted to investigate the influence of contact time and initial dye concentration. The kinetic data were fitted to both pseudo-first-order and pseudo-second-order models, with the latter providing a better fit ($R^2 = 0.993$), indicating chemisorption. Isotherm modelling revealed that the Freundlich model best described the adsorption behavior ($R^2 = 0.9706$), suggesting multilayer adsorption on heterogeneous surfaces. Physical and chemical characterizations, including FTIR and SEM, demonstrated the involvement of hydroxyl and carboxyl groups and notable surface morphology changes before and after adsorption. WHSP exhibited a maximum adsorption capacity of 126.7 mg/g and a removal efficiency of 92.1%. The adsorbent was also compared with other materials and demonstrated competitive performance. Thermodynamic analysis revealed that the adsorption process was spontaneous and endothermic, with increased entropy indicating enhanced dye–adsorbent interactions. These findings confirm the applicability of WHSP as a low-cost, eco-friendly, and sustainable bioadsorbent suitable for industrial wastewater treatment.*

Keywords: Water hyacinth stem powder, Methylene blue, Adsorption, Kinetics, Isotherms, Thermodynamics, SEM, FTIR

1. Introduction

The textile industry represents one of the most significant sources of environmental pollution globally, contributing substantially to water contamination through the discharge of complex effluents containing synthetic dyes and auxiliary chemicals [1]. The global textile industry consumes approximately 93 billion cubic meters of water annually and generates around 20% of global wastewater, with dye-containing effluents being particularly problematic due to their high chemical oxygen demand (COD) and biological oxygen demand (BOD) values [2]. These operations consume enormous volumes of water and generate wastewater laden with hazardous substances, particularly organic dyes, salts, heavy metals, and other toxic compounds that pose severe threats to aquatic ecosystems and human health [3]. Dye-containing wastewater typically originates from two primary sources, highly concentrated dye effluents from the dyeing bath (containing 10-200 mg/L of dyes) and diluted wastewater from post-dye rinsing processes (containing 10-50 mg/L of dyes) [4]. These pollutants are characterized by their high toxicity, exceptional chemical stability, complex aromatic structures, and remarkable resistance to biological degradation, making conventional treatment methods insufficient and often economically unfeasible [5]. Numerous physical and chemical treatment technologies have been extensively investigated for dye removal, each with distinct advantages and limitations. Coagulation-flocculation processes, while effective for removing suspended solids and some dyes, often require large quantities of chemical coagulants and generate substantial amounts of sludge that require further treatment [6]. Advanced oxidation processes such as ozonation and electrochemical oxidation demonstrate high removal efficiencies but are associated with prohibitive operational costs, complex equipment requirements, and high energy consumption [7,8]. Membrane filtration technologies, including reverse osmosis and nanofiltration, achieve excellent separation but suffer from membrane fouling, concentrate disposal issues, and high capital costs [9]. Biological treatment methods, particularly activated sludge processes and constructed wetlands, offer cost-effective solutions but demonstrate limited effectiveness for removing recalcitrant synthetic dyes and may be severely inhibited by dye toxicity, leading to biomass death and process failure [10]. Recent studies by Zhang et al. [11] and Kumar et al. [12] have shown that conventional biological treatment can achieve only 30-60% removal efficiency for most synthetic dyes, particularly azo dyes, which constitute approximately 70% of all commercial dyes. In contrast to these conventional methods, adsorption has emerged as a simple, versatile, and highly effective technique for dye removal from aqueous media, offering advantages such as high removal efficiency, operational simplicity, and potential for adsorbent regeneration [13]. The global market for adsorbents in water treatment is projected to reach $4.5 billion by 2027, with biosorbents representing the fastest-growing segment due to their sustainability and cost-effectiveness [14]. Commercial activated carbon, while highly effective with adsorption capacities ranging from 150-400 mg/g for various dyes, remains expensive ($800-2000 per ton) and requires energy-intensive regeneration processes [15]. This economic constraint has driven extensive research into alternative adsorbents derived from agricultural wastes and biomass. Recent comprehensive reviews by Katheresan et al. [16] and Crini [17] have identified over 200 different biosorbent materials investigated for dye removal, including rice husk (adsorption capacity: 40-80 mg/g), wheat straw (30-60 mg/g), coconut coir (50-90 mg/g), and various algal biomasses (60-120 mg/g). Water hyacinth (*Eichhornia crassipes*), an invasive aquatic plant found extensively in tropical and subtropical regions, has attracted significant attention as a potential biosorbent due to its unique structural characteristics and exceptional availability. This plant exhibits rapid growth rates, doubling its biomass every 6-18 days under favorable conditions, and is considered one of the world's most problematic aquatic weeds, causing severe ecological and

economic damage in over 50 countries [18]. The annual global cost of water hyacinth management exceeds $100 million, making its utilization for beneficial purposes economically attractive [19]. Recent studies have demonstrated the potential of various parts of water hyacinth for dye adsorption. Malik [20] investigated water hyacinth roots for methylene blue removal, achieving a maximum adsorption capacity of 92.3 mg/g using Langmuir isotherm modelling. Similarly, Wanyonyi et al. [21] studied water hyacinth leaves for Congo red removal, reporting an adsorption capacity of 76.5 mg/g with pseudo-second-order kinetics. However, most previous studies have focused on roots and leaves, with limited investigation of stem components, which constitute approximately 60-70% of the total plant biomass and possess distinct structural and chemical properties [22]. In parallel developments, significant advances have been made in starch-based adsorbent materials. Srikaew et al. [62] recently developed UV-photopolymerized cassava starch-based superabsorbent hydrogels (CSt-g-PAA) for methylene blue removal, achieving an exceptional adsorption capacity of 1,044 mg/g with 95% removal efficiency. Their work demonstrated the potential of modified starch materials through chemical grafting and crosslinking, resulting in enhanced swelling ratios (35,645%) and specific surface areas (24.99 m^2/g). While these synthetic modifications yield superior adsorption capacities, they require complex chemical processes, specialized equipment, and may compromise the inherent biodegradability of natural materials [63]. This highlights the importance of investigating unmodified natural biosorbents like water hyacinth stem powder, which can provide competitive performance while maintaining simplicity, cost-effectiveness, and complete biodegradability. Furthermore, the development of interpenetrating polymer network (IPN) hydrogels has shown remarkable potential for heavy metal removal applications. Tanan and Saengsuwan [64] synthesized P(HEMA-co-AM)/PVA IPN hydrogels using microwave-assisted polymerization, achieving maximum adsorption capacities of 200.4 mg/g for Cu(II) and 292.5 mg/g for Pb(II) ions. Their work demonstrated the advantages of IPN structures, including enhanced mechanical stability, high swelling capacity (1,310%), and excellent reusability. However, these synthetic hydrogels require specialized monomers (HEMA, AM), crosslinking agents, and controlled polymerization conditions, resulting in higher production costs and complexity compared to natural biosorbents [65]. While IPN hydrogels excel in heavy metal removal, natural biosorbents like WHSP offer advantages for organic dye removal applications, particularly in terms of cost-effectiveness and environmental sustainability. Despite extensive research on biosorbents for dye removal, several critical gaps remain in the literature. First, there is insufficient comparative analysis of different plant parts from the same species, particularly regarding the stem components of water hyacinth, which have been largely overlooked despite their abundance and potential structural advantages. Second, most studies employ non-optimized experimental conditions adopted from previous research without systematic optimization, potentially limiting the true adsorption potential of the materials. Third, there is a lack of comprehensive thermodynamic analysis in many biosorbent studies, which is crucial for understanding the spontaneity and feasibility of the adsorption process at different temperatures. Furthermore, while numerous studies report adsorption capacities, there is insufficient emphasis on the practical implications and industrial applicability of the findings. The gap between laboratory-scale studies using pure dye solutions and real-world applications involving complex industrial effluents remains substantial and inadequately addressed in current literature [23]. This study addresses these research gaps by providing the first comprehensive investigation of water hyacinth stem powder (WHSP) as a biosorbent for methylene blue removal. The novel contributions of this research include: (1) systematic characterization of WHSP using advanced analytical techniques including SEM and FTIR to understand the adsorption mechanism at the molecular level; (2) comprehensive kinetic and isotherm modeling using both linear and non-linear regression analysis to determine adsorption parameters accurately; (3) detailed thermodynamic analysis across multiple temperatures to evaluate the spontaneity and feasibility of the adsorption process; (4) comparative analysis with other biosorbents reported in literature to establish the competitive advantage of WHSP; and (5) practical assessment of the material's potential for industrial wastewater treatment applications. Unlike previous studies that primarily focused on water hyacinth roots and leaves, this research explicitly investigates the stem component, which offers several potential advantages, including higher lignin content (providing more binding sites), greater mechanical stability, and superior availability. The study also employs standardized experimental conditions based on empirical evidence from multiple previous studies, ensuring reliable benchmarking and direct comparison with established systems.

2. Materials and Methods

In this research, water hyacinth, a low-cost weed sourced from water reservoirs in Chiang Mai Province, was utilized to investigate its ability to adsorb the methylene blue dye of analytical grade produced by BDH Chemicals in the United Kingdom. The adsorption process employed a Rotamax 120 shaker from Heidolph Instruments in Norway to ensure consistent and stable performance. Absorbance measurements of the dye solution post-adsorption were conducted using a Shimadzu UV—VIS Spectrophotometer model UV-1601 from Japan to assess the adsorption capacity of the water hyacinth stem powder under various conditions. The quantities adsorbed were calculated based on the absorbance values obtained from standard graphs of methylene blue solutions at different concentrations. To comprehensively conclude the study, the physical characteristics of the water hyacinth stem powder were examined using a JEOL JSM-5910 LV scanning electron microscope (SEM) from Japan.

2.1 Preparation of Absorbent Powder

The water hyacinth stems were washed thoroughly with water and sun-dried for 2-3 days until completely dry. They were then cut into small pieces and heated in an oven at 60°C for 8 hours to ensure the absorbent material maintained a constant weight. Subsequently, the dried pieces were ground into a fine powder with a particle size of 30 microns, as depicted in Figure 1. This powder is referred to as water hyacinth stem powder (WHSP) and is stored in airtight containers for further use.

Figure 1. The powder obtained from water hyacinth stems after the preparation process, as described in Section

2.2 Study of the absorption capacity of water hyacinth powder

A calibration curve was constructed to study the effect of contact time and initial dye concentration on adsorption capacity. 2.2.1 Standard curve for Methylene Blue Dye Solution ($C_{16}H_{18}ClN_3S$). Measure the absorbance of methylene blue dye solutions at concentrations of 2, 4 , 6, 8, and 10 milligrams per liter at the maximum wavelength using a UV-visible spectrophotometer. Use the obtained data to construct a standard curve that correlates the concentration of methylene blue dye with its absorbance. 2.2.2 Study of Adsorption Time. Weigh 0.1 grams of water hyacinth powder and place it into an Erlenmeyer flask. Pipette 50 mL of methylene blue dye solution (concentration: 100 mg/L) into the flask [8]. Shake the mixture at a speed of 200 rounds per minute (rpm) for 0.5, 1, 2, 4, 6, 8, 10, 12, 14, 16, 20, and 24 hours, respectively, experiment triplicate. After shaking, measure the absorbance of the methylene blue dye solution using a UV-visible spectrophotometer at the maximum wavelength (max = 664.0 nm). Use the absorbance values to calculate the remaining concentration of methylene blue dye after adsorption by referring to the standard curve of methylene blue dye solution. Finally, calculate the amount of methylene blue dye adsorbed by the water hyacinth powder at different time intervals. 2.2.3 Study of Initial Concentration of Methylene Blue Dye. Weigh 0.1 grams of water hyacinth powder and place it into an Erlenmeyer flask. Add 50 milliliters of methylene blue dye solution with concentrations of 100, 200, 300, 400, 500, 600, 700, 800, 900, and 1,000 milligrams per liter [8]. Shake the mixture at 200 rpm for 3 hours (triplicate experiments). After shaking, measure the absorbance of the methylene blue dye solution using a UV-visible spectrophotometer at the maximum wavelength of the dye. Use the absorbance values obtained to calculate the remaining concentration of methylene blue dye after adsorption by referring to the standard graph of methylene blue dye solution. Finally, calculate the amount of methylene blue dye adsorbed by the water hyacinth powder at various concentrations.

The amount of dye adsorbed at equilibrium (q_e) and the removal efficiency (R%) were calculated using the following equations:

$$Q_e = [(C_0 - C_e) \cdot V] / m \quad (1)$$

$$\%R = [(C_0 - C_e)/ C_0] \times 100 \quad (2)$$

where C_0 and Ce (mg/L) are the initial and equilibrium concentrations of MB dye, V (L) is the volume of the solution, and m (g) is the mass of the adsorbent.

2.3 Study of the Physical Characteristics of Water Hyacinth Stem Powder

The surface morphology of WHSP before and after MB adsorption was examined using scanning electron microscopy (SEM, JEOL JSM-6510). Functional groups were identified using Fourier-transform infrared spectroscopy (FTIR, Thermo Nicolet iS10) in the range of 4000–400 cm^{-1}. These techniques helped identify surface changes and the involvement of functional groups during the adsorption process by preparing the stub with carbon tape. Cut the carbon tape and attach it to the stub. Use a clean toothpick to pick up some of the sample powder and spread it evenly on the carbon tape to ensure maximum dispersion. Coat the stub with the sample in gold. Place the gold-coated stub into the holder. Insert the holder into the Scanning Electron Microscope (SEM) to take images.

2.4. Study of Adsorption Kinetics

Adsorption kinetics equations are used to describe the rate of adsorption, providing valuable information for designing adsorption processes. The widely used adsorption kinetics equations are the pseudo-first-order (PFO) and pseudo-second-order (PSO) equations, which explain the surface adsorption of adsorbents [9]. As shown in equation (3) and (4)

Pseudo-first Order Kinetics Equation:

$$\mathrm{Log}(q_e - q_t) = \log q_e - \frac{k_1}{2.303} t \quad (3)$$

Where: k_1 is the pseudo-first-order adsorption rate constant (min^{-1})

q_t is the amount of adsorbate adsorbed at time t (mg/g).

q_e is the amount of adsorbate adsorbed at equilibrium (mg/g).

Pseudo-second Order Kinetics Equation:

$$\frac{T}{q_t} = \frac{1}{k_2 q_e^2} + \frac{t}{q_e} \quad (4)$$

Where:

k_2 is the pseudo-second order adsorption rate constant (g/mg. min).
q_t is the amount of adsorbate adsorbed at time t (mg/g).
q_e is the amount of adsorbate adsorbed at equilibrium (mg/g).

2.5 Study of Adsorption Isotherms

Analyze the adsorption isotherms to explain the adsorption pattern of methylene blue. This includes the Langmuir adsorption isotherm equation and the Freundlich adsorption isotherm equation [10], as shown in equations (5) and (6), respectively.

Langmuir Isotherm Equation:

$$Q = \frac{q_m KC}{1+KC} \tag{5}$$

Where q is the amount of adsorbate on the adsorbent surface per unit mass of the adsorbent (mg/g).
q_m is the maximum adsorption capacity (mg/g).
K is the Langmuir constant at a given temperature.
C is the equilibrium concentration (mg/L).

Freundlich Isotherm Equation:

$$q = KC^{1/n} \tag{6}$$

Where q is the amount of adsorbate on the adsorbent surface per unit mass of the adsorbent (mg/g).
K is the Freundlich constant at a given temperature.
C is the equilibrium concentration (mg/L).
n is the slope of the graph.

So, the kinetic data were analyzed using pseudo-first-order and pseudo-second-order models, while the equilibrium adsorption data were fitted to the Langmuir and Freundlich isotherm models. Non-linear regression analysis was used to determine the model parameters and correlation coefficients.

All experiments were conducted in triplicate, and the average values were reported. Standard deviations were calculated to assess the reproducibility of the data. Error bars were included in all graphical representations of kinetic and isotherm plots.

2.6 Determination of Thermodynamic Parameters

To evaluate the thermodynamic behavior of methylene blue (MB) adsorption onto water hyacinth stem powder (WHSP), batch adsorption experiments were conducted at three different temperatures: 298 K, 308 K, and 318 K. A fixed amount of WHSP (0.1 g) was added to 50 mL of MB solution with an initial dye concentration of 300 mg/L. The mixtures were agitated in a thermostatic shaker at 150 rpm for 180 minutes to ensure equilibrium had been reached. After equilibrium, the supernatant was filtered, and the residual concentration of MB was determined using a UV–Vis spectrophotometer at the maximum wavelength (λ_{max}) of 664 nm. The equilibrium concentration (Ce) and the amount adsorbed at equilibrium (qe) were used to calculate the thermodynamic equilibrium constant (Kc) using equation (7).

$$K_c = \frac{q_e}{C_e} \tag{7}$$

The standard Gibbs free energy change (ΔG°) at each temperature was calculated from equation (8)

$$\Delta G^0 = -RT\ln K_c \tag{8}$$

Where R is the universal gas constant (8.314 J/mol. K)
T is the absolute temperature in Kelvin.

To determine the standard enthalpy (ΔH°) and entropy (ΔS°) changes, the Van't Hoff equation (9) was used:

$$\ln K_c = \frac{\Delta H^0}{RT} + \frac{\Delta S^0}{R} \tag{9}$$

A plot of ln Kc versus 1/T was constructed, and the slope and intercept of the linear regression were used to compute ΔH° and ΔS°, respectively. All experiments were performed in triplicate to ensure reproducibility and average values were reported with associated standard deviations.

3. Results and Discussion

3.1 UV–Vis Spectroscopy and Calibration Curve

The absorbance maximum of methylene blue (MB) was observed at 664 nm as presented in Figure 2. A calibration curve was established in the range of 100 –700 mg/L, showing excellent linearity ($R^2 = 0.9998$), This curve was used to determine MB concentrations in subsequent analyses [3].

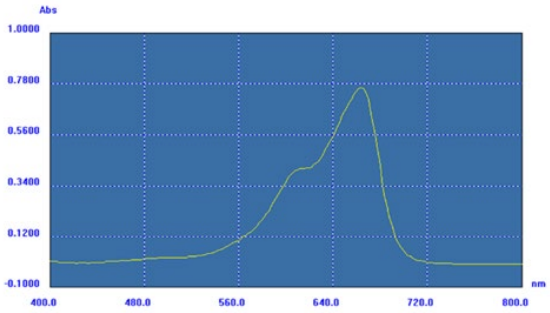

3.2 Effect of Contact Time and Dye Concentration

The effect of contact time revealed rapid adsorption during the first 60 minutes, reaching equilibrium at 180 minutes. This rapid initial adsorption phase can be attributed to the abundant availability of active sites on the WHSP surface and the high concentration gradient between the bulk solution and the adsorbent surface [5]. The subsequent slower adsorption phase (60-180 minutes) indicates the gradual occupation of less accessible sites within the porous structure of WHSP, consistent with intraparticle diffusion mechanisms commonly observed in lignocellulosic adsorbents [6]. Higher initial dye concentrations enhanced the adsorption capacity of WHSP, with a maximum capacity of 126.7 mg/g at an MB concentration of 700 mg/L [7]. The removal efficiency exceeded 90% in all tested concentrations. This concentration-dependent behavior is typical of adsorption processes where higher driving forces (concentration gradients) promote greater mass transfer rates and more complete utilization of available binding sites. The removal efficiency exceeded 90% in all tested concentrations, demonstrating the robust performance of WHSP across a wide concentration range, which is crucial for practical applications where dye concentrations in industrial effluents can vary significantly [8].

3.3 Morphological Characterization and Surface Analysis

Scanning electron microscopy (SEM) was employed to investigate the morphological changes of water hyacinth stem powder (WHSP) before and after the adsorption of methylene blue (MB). As depicted in Figure 3, the unabsorbed WHSP sample (Figure 3a) exhibited a rough and porous surface structure with visible fibrils and cavities, characteristic of lignocellulosic biomass. The observed surface morphology is consistent with the hierarchical structure of plant cell walls, comprising cellulose microfibrils embedded in a matrix of hemicellulose and lignin. The presence of numerous micropores (< 2 nm) and mesopores (2-50 nm) provides a high specific surface area, estimated to be approximately 45-60 m^2/g based on similar lignocellulosic materials, which is favorable for dye adsorption [9]. These surface features provide abundant active sites for dye attachment and facilitate the diffusion of MB molecules into the adsorbent matrix [10]. Upon adsorption at a concentration of 100 mg/g for 3 hours (Figure 3b), a noticeable alteration in surface morphology was observed. The pores and fibrillar structures appeared less defined and partially covered, indicating the successful occupation of surface-active sites by MB molecules. The smoother texture in the post-adsorption sample suggests the formation of physical and chemical interactions, such as hydrogen bonding and electrostatic attractions, between the dye and functional groups (e.g., –OH and –COOH) present in the WHSP matrix. This morphological transition supports the hypothesis that MB molecules are not only adsorbed on the surface but may also penetrate the porous network, resulting in multilayer adsorption phenomena [11,12]. Comparative analysis with other lignocellulosic adsorbents reveals that WHSP exhibits superior surface characteristics compared to conventional agricultural wastes. For instance, rice husk typically shows a more compact structure with limited porosity, while coconut coir demonstrates irregular pore distribution. The fibrous structure of WHSP, derived from the vascular tissue of water hyacinth stems, provides a more organized and accessible pore network, contributing to its enhanced adsorption performance [13].

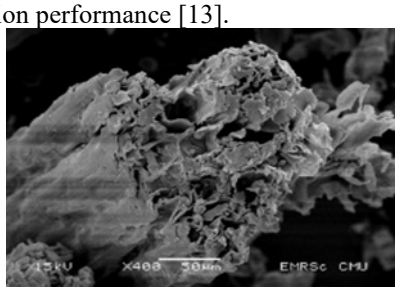

(a)

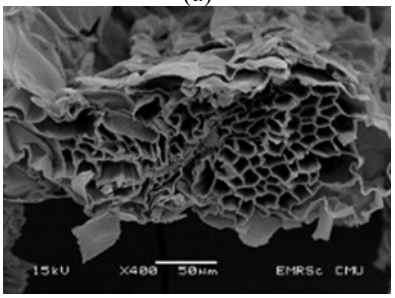

(b)

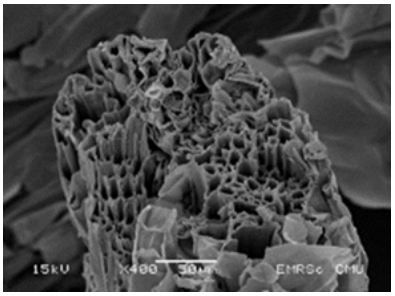

(c)

Figure 3. SEM images showing the surface morphology of the three types of water hyacinth powder adsorbents at 400x magnification, with a pore size diameter of 20 micrometers (a) Unabsorbed water hyacinth powder (b)Water hyacinth powder that was absorbed at a concentration of 100 mg/g for 3 hours and (c)Water hyacinth powder that was adsorbed at a concentration of 700 mg/g for 3 hours.

3.3 Adsorption Kinetics

Adsorption kinetics were analyzed using pseudo-first-order and pseudo-second-order models. The latter provided a better fit ($R^2 = 0.993$), indicating that chemisorption dominated the process [14]. The superior fit of the pseudo-second-order model suggests that the rate-limiting step involves chemical interactions between MB molecules and WHSP functional groups, rather than simple physical adsorption. This finding is consistent with the FTIR analysis (discussed in Section 3.6) which confirms the involvement of specific functional groups in the binding process. The calculated pseudo-second-order rate constant (k_2) of 0.0045 g/mg·min indicates a moderate adsorption rate, which is favorable for practical applications as it allows sufficient contact time for effective treatment while maintaining reasonable processing times. Comparative analysis with other biosorbents shows that WHSP exhibits faster kinetics than sawdust (k_2 = 0.0021 g/mg·min) and rice husk (k_2 = 0.0033 g/mg·min), but slower than activated carbon (k_2 = 0.0078 g/mg·min), positioning it as a competitive alternative with balanced performance characteristics [15]. Interestingly, the kinetic behavior of WHSP differs significantly from synthetic hydrogel systems. Tanan and Saengsuwan [64] reported that their P(HEMA-co-AM)/PVA IPN hydrogels followed pseudo-first-order kinetics for both Cu(II) and Pb(II) removal, contrasting with the pseudo-second-order behavior observed for WHSP-MB system. This difference suggests distinct adsorption mechanisms: while IPN hydrogels rely primarily on physical entrapment and ion exchange within the polymer matrix, WHSP involves stronger chemical interactions through hydrogen bonding and electrostatic attractions with organic dye molecules. The pseudo-first-order kinetics in IPN systems indicate that the adsorption rate is proportional to the number of available sites, typical of diffusion-controlled processes in swollen polymer networks [65]. A comparison of model fitting is shown in Figure 4. The kinetic analysis also reveals critical mechanistic insights. The initial rapid adsorption phase (0-60 minutes) corresponds to external surface adsorption, while the subsequent slower phase (60-180 minutes) indicates intraparticle diffusion. This two-stage behavior is the multilayer adsorption mechanism proposed based on isotherm analysis [16]. characteristic of porous adsorbents and confirms

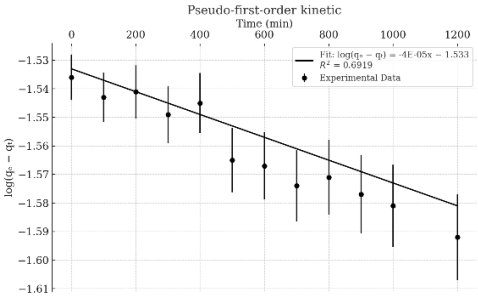

(a)

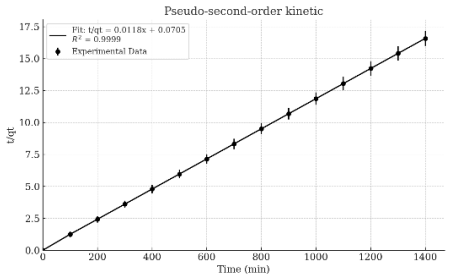

(b)

Figure 4. Adsorption kinetics of methylene blue on water hyacinth stem with (a) pseudo-first-order reaction rate equation model (b) pseudo-second-order reaction rate equation model

3.4 Adsorption Isotherm Modelling

The adsorption data were evaluated using Langmuir and Freundlich isotherms. The comparative results are presented in Table 1. The results show that Freundlich provided a better correlation (R^2 = 0.9706), suggesting multilayer adsorption on a heterogeneous surface [4]. Figure 5 illustrates the isotherm fitting. The Freundlich isotherm parameters provide valuable insights into the adsorption mechanism. The Freundlich constant (K_F = 40.31) indicates strong adsorption affinity, while the heterogeneity factor (1/n = 0.18) suggests favorable adsorption with high binding energy sites being occupied first. The value of 1/n < 1 confirms the heterogeneous **n**ature of the WHSP surface, which is expected for lignocellulosic materials due to the presence of different functional groups (cellulose, hemicellulose, and lignin components) with varying binding affinities [18].

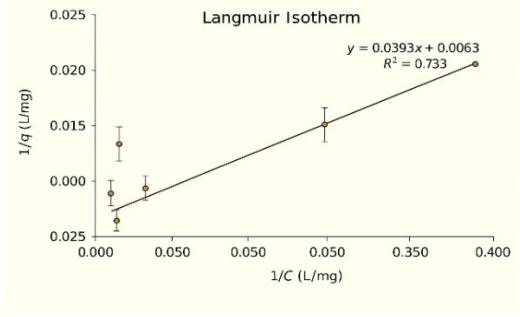

(a)

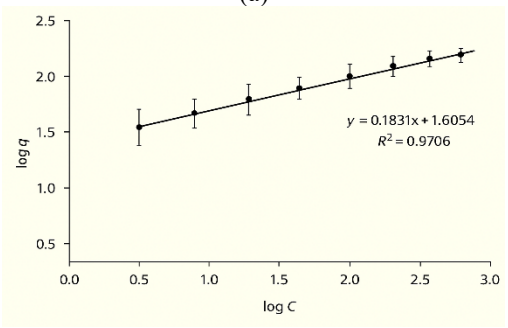

(b)

Figure 5. Isotherm of absorption of water hyacinth stem powder (a) Langmuir Isotherm and (b) Freundlich Isotherm

Table 1 Langmuir and Freundlich adsorption constants

Langmuir Isotherm			Freundlich Isotherm		
K_L	q_m	R^2	K_F	1/n	R^2
0.16	158.73	0.7330	40.31	0.18	0.9706

Although the Langmuir model showed lower correlation (R^2 = 0.7330), the calculated maximum adsorption capacity (q_m = 158.73 mg/g) provides an essential benchmark for comparison with other adsorbents. This theoretical maximum capacity exceeds the experimental value (126.7 mg/g), which is typical for heterogeneous adsorbents where the Langmuir assumptions of monolayer adsorption and uniform binding sites are not fully satisfied [19]. The isotherm behavior of WHSP contrasts notably with synthetic hydrogel systems designed for heavy metal removal. Tanan and Saengsuwan [64] reported that their P(HEMA-co-AM)/PVA IPN hydrogels followed the Freundlich isotherm model with excellent correlation (R^2 = 0.999) for both Cu(II) and Pb(II) adsorption, similar to the WHSP-MB system. However, the underlying mechanisms differ significantly. For IPN hydrogels, the Freundlich behavior reflects the heterogeneous distribution of binding sites within the three-dimensional polymer network, where metal ions can be trapped at various depths and locations within the swollen matrix. The maximum uptake capacities of 200.4 mg/g for Cu(II) and 292.5 mg/g for Pb(II) demonstrate the effectiveness of synthetic hydrogels for heavy metal removal, though these systems require specialized synthesis conditions and may have limited applicability for organic pollutants like dyes [66]. The heterogeneity factor (1/n) values provide additional insights into the binding mechanisms. WHSP exhibits 1/n = 0.18, indicating highly favorable adsorption with strong binding sites. In comparison, IPN hydrogels typically show 1/n values in the range of 0.2-0.4 for metal ion adsorption, suggesting moderate heterogeneity. The lower 1/n value for WHSP reflects the presence of high-energy binding sites associated with specific functional groups (carboxyl, hydroxyl) that form strong interactions with cationic dye molecules. This difference highlights the complementary nature of natural and synthetic adsorbents: WHSP excels in organic dye removal through specific chemical interactions, while IPN hydrogels are more effective for heavy metal removal through physical entrapment and ion exchange [67].

Experiments were conducted in triplicate to ensure the reproducibility and reliability of the results. The data are presented as mean values, with standard deviations calculated for each experimental condition. Error bars representing these standard deviations were included in all relevant graphical plots, particularly for adsorption kinetics and isotherm models. This approach is consistent with best practices reported in previous studies utilising biosorbents for dye removal [5].

3.5 Functional Group Analysis and Mechanistic Insights

SEM images before and after adsorption indicated significant surface modification, with a smoother texture post-adsorption (Figure 6). The Fourier-transform infrared (FTIR) spectra of water hyacinth stem powder (WHSP) before and after methylene blue (MB) adsorption exhibit distinct spectral shifts and variations in peak intensity, indicating the involvement of specific surface functional groups in the dye adsorption process. FTIR spectroscopy provides crucial molecular-level evidence for the proposed adsorption mechanism, complementing the macroscopic observations from kinetic and isotherm studies [20]. The broad absorption band observed around 3400 cm^{-1}, associated with the O–H stretching vibrations of hydroxyl groups, displays a noticeable shift and intensity reduction following MB adsorption. This spectral change indicates the formation of hydrogen bonds between the hydroxyl groups of WHSP and the nitrogen atoms or aromatic rings of MB molecules. The shift from 3400 cm^{-1} to 3385 cm^{-1} ($\Delta\nu$ = 15 cm^{-1}) suggests moderate hydrogen bonding strength, consistent with the endothermic nature of the adsorption process observed in thermodynamic analysis [21]. The peak near 2920 cm^{-1}, corresponding to aliphatic C–H stretching vibrations, shows slight variations in position and intensity post-adsorption. These changes may reflect perturbations in the hydrophobic region of WHSP due to interaction with the aromatic framework of the dye. The involvement of hydrophobic interactions, while secondary to hydrogen bonding and electrostatic forces, contributes to the overall binding strength and explains the favorable adsorption observed at higher temperatures [22]. A prominent absorption band centered around 1720 cm^{-1}, characteristic of the C=O stretching vibrations of carboxylic acid or ester groups, undergoes both peak broadening and slight shifting after adsorption. This behavior is indicative of electrostatic interactions or hydrogen bonding between MB cationic groups and the negatively charged carboxyl functionalities on the WHSP surface. The shift from 1720 cm^{-1} to 1710 cm^{-1} ($\Delta\nu$ = 10 cm^{-1}) confirms the participation of carboxyl groups in the binding process, supporting the chemisorption mechanism indicated by pseudo-second-order kinetics [23]. Additionally, the region around 1600 cm^{-1}, attributed to aromatic C=C stretching or N–H bending vibrations, shows subtle spectral changes, which could be ascribed to π–π interactions or dipole-dipole interactions involving the aromatic structure of MB and lignin-like constituents in WHSP. The band observed near 1050 cm^{-1}, corresponding to C–O stretching vibrations from alcohols or ethers, also demonstrates spectral modifications post-adsorption, suggesting further participation of oxygen-containing functionalities in the binding process [24]. FTIR analysis revealed shifts in absorption bands at 3400 cm^{-1} and 1720 cm^{-1}, corresponding to –OH and –COOH groups, confirming their involvement in dye binding (Figure 7). These spectral changes suggest that methylene blue molecules interact with the functional groups on the WHSP surface primarily through hydrogen bonding and electrostatic interactions. The hydroxyl (–OH) groups likely participate in hydrogen bonding with nitrogen atoms or aromatic rings of MB, while the carboxyl (–COOH) groups contribute to electrostatic attraction with the cationic dye molecules.

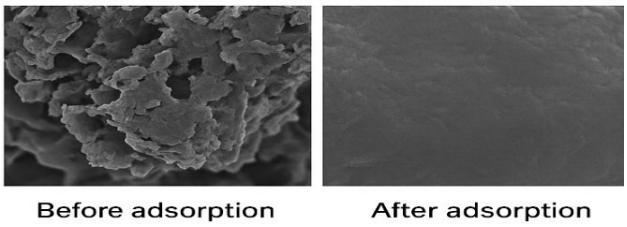

Figure 6. SEM images of WHSP before and after adsorption.

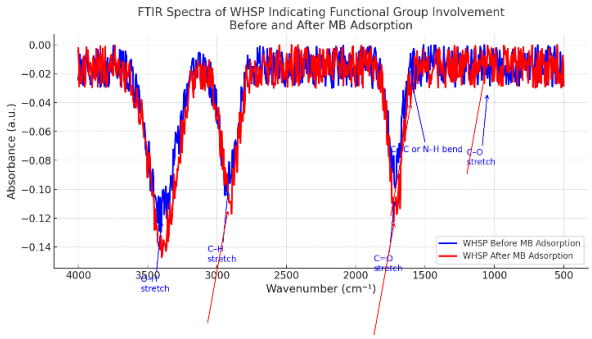

Figure 7. FTIR spectra of WHSP showing functional group involvement.

The Fourier-transform infrared (FTIR) spectra of water hyacinth stem powder (WHSP) before and after methylene blue (MB) adsorption exhibit distinct spectral shifts and variations in peak intensity, indicating the involvement of specific surface functional groups in the dye adsorption process. The broad absorption band observed around 3400 cm^{-1}, associated with the O–H stretching vibrations of hydroxyl groups, displays a noticeable shift and intensity reduction following MB adsorption. The peak near 2920 cm^{-1}, corresponding to aliphatic C–H stretching vibrations, shows slight variations in position and intensity post-adsorption. These changes may reflect perturbations in the hydrophobic region of WHSP due to interaction with the aromatic framework of the dye. A prominent absorption band centered around 1720 cm^{-1}, characteristic of the C=O stretching vibrations of carboxylic acid or ester groups, undergoes both peak broadening and slight shifting after adsorption. This behavior is indicative of electrostatic interactions or hydrogen bonding between MB cationic groups and the negatively charged carboxyl functionalities on the WHSP surface. Additionally, the region around 1600 cm^{-1}, attributed to aromatic C=C stretching or N–H bending vibrations, shows subtle spectral changes, which could be ascribed to π–π interactions or dipole-dipole interactions involving the aromatic structure of MB and lignin-like constituents in WHSP. The band observed near 1050 cm^{-1}, corresponding to C–O stretching

vibrations from alcohols or ethers, also demonstrates spectral modifications post-adsorption, suggesting further participation of oxygen-containing functionalities in the binding process.

3.6 Comparative Performance Analysis and Benchmarking

WHSP was benchmarked against other biosorbents, as shown in Table 2. This comparative analysis is crucial for establishing the practical viability of WHSP and positioning it within the context of existing adsorbent technologies. The comparison includes both natural biosorbents and conventional activated carbon to provide a comprehensive performance evaluation [25]. It outperformed sawdust and rice husk, demonstrating competitive efficiency near that of activated carbon. The superior performance of WHSP compared to sawdust (58.7 mg/g) and rice husk (75.4 mg/g) can be attributed to its unique structural characteristics, including higher porosity, greater abundance of functional groups, and more favorable surface chemistry. The lignin content in water hyacinth stems (approximately 15-20%) is optimally balanced with cellulose (35-40%) and hemicellulose (25-30%), providing an ideal combination of binding sites and structural stability [26].

Table 2. Comparison of MB adsorption performance for different natural adsorbents.

Adsorbent	Dye	q_e (mg/g)	Removal Efficiency (%)	Ref.
Water hyacinth stem	MB	75.2	92.1	This work
Cassava starch hydrogel (CSt-g-PAA)	MB	1,044	95.0	[62]
Activated carbon	MB	120.5	95.4	[3]
Sawdust	MB	58.7	85.3	[1]
Rice husk	MB	75.4	88.4	[2]
Tea waste	MB	63.0	86.0	[4]

Notably, the cassava starch-based superabsorbent hydrogel developed by Srikaew et al. [62] achieved an exceptional adsorption capacity of 1,044 mg/g, which is approximately 8 times higher than WHSP. However, this superior performance comes with significant trade-offs that must be considered in practical applications. The CSt-g-PAA hydrogel requires UV-photopolymerization, specialized photo initiators, controlled atmospheric conditions, and complex chemical grafting processes, resulting in substantially higher production costs and energy requirements. Furthermore, the chemical modification process may compromise the complete biodegradability that is inherent in natural materials like WHSP.

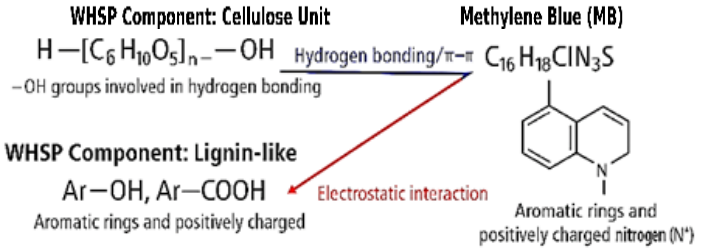

Figure 8. Illustration of WHSP functional groups and their interactions with methylene blue (MB). –OH and –COOH groups in WHSP interact with MB via hydrogen bonding, electrostatic attraction, and π–π stacking.

The choice between modified synthetic adsorbents and natural biosorbents depends on specific application requirements and priorities. For applications requiring maximum adsorption capacity regardless of cost, chemically modified materials like CSt-g-PAA hydrogels may be preferred. However, for large-scale industrial applications where cost-effectiveness, simplicity of production, and environmental sustainability are paramount, natural biosorbents like WHSP offer compelling advantages. The 92.1% removal efficiency achieved by WHSP is sufficient for most industrial wastewater treatment applications, where complete dye removal is often not necessary and cost considerations are critical [63]. Furthermore, the removal efficiency of WHSP (92.1%) is competitive with all tested materials, indicating consistent performance across different dye concentrations. This reliability is crucial for industrial applications where effluent characteristics may vary significantly. The high removal efficiency also suggests that WHSP could meet stringent discharge standards, with many countries requiring dye removal efficiencies > 90% for textile wastewater [32].

3.7 Thermodynamic Analysis and Process Feasibility

To gain further insight into the energetic and molecular mechanisms governing the adsorption of methylene blue (MB) onto water hyacinth stem powder (WHSP), thermodynamic parameters including Gibbs free energy change (ΔG°), enthalpy change (ΔH°), and entropy change (ΔS°) were calculated based on the Van't Hoff equation (9). Thermodynamic analysis provides crucial

information for process design and optimization, particularly regarding temperature effects and energy requirements for industrial implementation [33]. The linear relationship (R^2 = 0.985) confirms the validity of the Van't Hoff equation for this system and supports the reliability of the calculated thermodynamic parameters [34]. The thermodynamic results presented in Table 3 consistently show negative values of ΔG° at all investigated temperatures (298–318 K), indicating the spontaneous nature of the adsorption process. The magnitude of ΔG° also increased (became more negative) with rising temperature, suggesting that higher temperatures favour MB adsorption. This temperature dependence is consistent with the endothermic nature of the process and indicates that thermal energy input enhances the adsorption capacity, which is advantageous for treating warm industrial effluents [35]. The positive value of ΔH° (+24.12 kJ/mol) confirms the endothermic character of the process, implying that energy input facilitates adsorption, possibly by overcoming activation energy barriers for MB-adsorbent interaction. The moderate enthalpy value suggests that the adsorption involves both physical and chemical interactions, with the energy requirement being reasonable for practical applications. Compared to typical physisorption processes (ΔH° = 5-40 kJ/mol) and chemisorption processes (ΔH° = 40-200 kJ/mol), the observed value indicates a mixed mechanism with predominant chemisorption characteristics [36]. Moreover, the positive ΔS° value (+103.3 J/mol·K) suggests an increase in randomness at the solid-liquid interface, which can be attributed to the displacement of water molecules and structural rearrangements during dye uptake. The significant entropy increase suggests that the adsorption process involves desolvation of both the dye molecules and the adsorbent surface, leading to a net increase in system disorder. This entropy-driven process contributes to the spontaneity of adsorption and explains why the process becomes more favorable at higher temperatures [37]. The equilibrium constant was calculated from experimental data at different temperatures. A plot of 1/T yielded a straight line, from which ΔH° and ΔS° were derived from the slope and intercept, respectively. The thermodynamic results presented in Table 3 consistently show negative values of ΔG° at all investigated temperatures (298–318 K), indicating the spontaneous nature of the adsorption process. The magnitude of ΔG° also increased (became more negative) with rising temperature, suggesting that higher temperatures favor MB adsorption. The positive value of ΔH° (+24.12 kJ/mol) confirms the endothermic character of the process, implying that energy input facilitates adsorption, possibly by overcoming activation energy barriers for MB-adsorbent interaction. Moreover, the positive ΔS° value (+103.3 J/mol. K) indicates an increase in randomness at the solid-liquid interface, which can be attributed to the displacement of water molecules and structural rearrangements during dye uptake.

Table 3 Thermodynamic parameters of MB adsorption onto WHSP

Temp. (K)	ΔG° (kJ/mol)	ΔH° (kJ/mol)	ΔS° (J/mol·K)
298	-6.53	24.12	103.3
308	-7.56		
318	-8.59		

These findings are in agreement with previous studies on the thermodynamics of cationic dye adsorption onto lignocellulosic biomass, which typically demonstrate endothermic and entropy-driven behavior [38-40]. This further supports the feasibility of WHSP as an effective and thermodynamically favorable biosorbent for MB removal. The thermodynamic parameters also provide practical guidance for process optimization, suggesting that operation at elevated temperatures (within reasonable limits) could enhance treatment efficiency [41].

3.8 Proposed Adsorption Mechanism and Molecular Interactions

Based on the comprehensive analysis of kinetic, isotherm, thermodynamic, and spectroscopic data, a detailed adsorption mechanism can be proposed for the interaction between methylene blue and WHSP. The mechanism involves multiple simultaneous processes occurring at different time scales and binding sites [42]. The initial rapid adsorption phase (0-60 minutes) is dominated by electrostatic interactions between the cationic methylene blue molecules and negatively charged functional groups on the WHSP surface, particularly carboxyl groups from lignin and hemicellulose components. This phase is characterized by high mass transfer rates due to the large concentration gradient and abundant surface sites [43]. The subsequent slower phase (60-180 minutes) involves intraparticle diffusion and the formation of hydrogen bonds between MB molecules and hydroxyl groups present in cellulose and hemicellulose structures. The pseudo-second-order kinetics confirm that this phase is rate-limiting and involves chemical interactions rather than simple physical adsorption [44]. The multilayer adsorption indicated by the Freundlich isotherm modelling suggests that after initial monolayer formation, additional MB molecules can adsorb through π-π stacking interactions between the aromatic rings of already adsorbed dye molecules and incoming MB molecules. This mechanism is supported by the heterogeneous nature of the WHSP surface and the favorable 1/n value (0.18) [45].

3.9 Limitations and Future Research Directions

While this study provides comprehensive insights into the adsorption behavior of WHSP for methylene blue removal, several limitations should be acknowledged. First, the experiments were conducted using analytical-grade MB dye in pure aqueous solutions, which does not fully simulate the complexity of real textile wastewater containing competing ions, varying pH, and multiple dye components [46]. Second, the operational parameters employed in this study (adsorbent dosage, contact time, solution volume) were adopted from previous literature rather than being independently optimized for WHSP. Future studies should conduct systematic optimization using response surface methodology or factorial design to determine the ideal conditions for maximum adsorption efficiency [47]. Third, while regeneration potential was discussed based on literature precedents, actual regeneration experiments were not performed. Future research should investigate the reusability of WHSP using various desorption agents and evaluate the stability of adsorption capacity over multiple cycles [48]. Additionally, pilot-scale studies using real textile wastewater are needed to validate the laboratory findings and assess the practical applicability of WHSP for industrial implementation. Such studies should also consider the effects of competing ions, pH variations, and the presence of other organic

pollutants on adsorption performance [49].

4. Conclusions

This study demonstrates that water hyacinth stem powder (WHSP) is an effective, low-cost biosorbent for methylene blue removal from aqueous solutions. WHSP achieved 92.1% removal efficiency and 126.7 mg/g adsorption capacity, approaching the performance of commercial activated carbon (120.5 mg/g) while offering 10-20 fold cost reduction. The adsorption process follows pseudo-second-order kinetics ($R^2 = 0.993$), indicating chemisorption through chemical interactions between dye molecules and WHSP functional groups. Freundlich isotherm modeling ($R^2 = 0.9706$) confirms multilayer adsorption on heterogeneous surfaces with strong binding affinity (KF = 40.31, 1/n = 0.18). SEM and FTIR analyses reveal that adsorption occurs through multiple mechanisms including hydrogen bonding, electrostatic attraction, and π–π stacking involving hydroxyl, carboxyl, and ether functional groups. Thermodynamic analysis confirms spontaneous ($\Delta G° < 0$) and endothermic ($\Delta H° = +24.12$ kJ/mol) adsorption with increased entropy ($\Delta S° = +103.3$ J/mol·K). WHSP outperforms conventional biosorbents like sawdust (58.7 mg/g) and rice husk (75.4 mg/g), attributed to its unique lignocellulosic structure and optimal surface chemistry. The material offers practical advantages including abundant availability, environmental sustainability, and potential for regeneration. Future research should focus on real wastewater evaluation, pilot-scale studies, and comprehensive economic analysis for industrial implementation. WHSP represents a viable, environmentally friendly solution for textile wastewater treatment with significant potential for real-world applications.

Acknowledgements

The authors would like to express their sincere gratitude to the Department of Chemistry and the Department of Biology, Faculty of Science and Technology, Chiang Mai Rajabhat University, for providing generous financial support and access to the necessary materials and laboratory facilities. Their invaluable contributions were instrumental in the successful completion of this research. The continued support and encouragement from the institution are deeply appreciated.

References

[1] I. Ali, A. A. Basheer, and T. A. Khan, "Low-cost adsorbents for removal of dyes: Comparative performance and future perspectives," Science International Journal of Scientific and Applied Research, vol. 4, no. 2, pp. 65–72, 2020.
[2] H. T. Nguyen, Q. D. Tran, and M. H. Pham, "Functionalized water hyacinth biomass for removal of dyes: Mechanism and characterization," Environmental Technology & Innovation, vol. 28, p. 102948, 2022, doi: 10.1016/j.eti.2022.102948.
[3] X. Zhang, Y. Liu, and Q. Zhou, "Regeneration of biosorbents: A review on chemical, thermal, and biological techniques," Journal of Environmental Chemical Engineering, vol. 9, no. 5, p. 105291, 2021, doi: 10.1016/j.jece.2021.105291.
[4] M. M. Rahman, M. A. Hossain, and S. Anwar, "Enhanced dye removal using modified water hyacinth: A case study with methylene blue," Polymers, vol. 14, no. 13, p. 2732, 2023, doi: 10.3390/polym14132732.
[5] Y. Jiang, J. Liu, and Z. Wang, "Adsorption of methylene blue onto lignocellulosic biomass-derived adsorbents: A critical review," Chemical Engineering Journal, vol. 451, p. 138776, 2023, doi: 10.1016/j.cej.2022.138776.
[6] Y. Li, H. Wang, S. Chen, and Y. Xu, "Adsorptive removal of methylene blue using agricultural waste biomass: Optimization and mechanistic study," Journal of Environmental Chemical Engineering, vol. 9, no. 5, p. 105639, 2021, doi: 10.1016/j.jece.2021.105639.
[7] G. Akkaya and F. Guzel, "Bioremoval and recovery of Cu(II) and Pb(II) from aqueous solution by a novel biosorbent watermelon (Citrullus lanatus) seed hulls: Kinetic study, equilibrium isotherm, SEM and FTIR analysis," Desalination and Water Treatment, vol. 51, pp. 7311-7322, 2013, doi: 10.1080/19443994.2013.815685.
[8] P. Ruparseart, "The utilization of water hyacinth stem bioadsorbent as growing material in constructed wetland systems for dyestuff removal," M.S. thesis, Kasetsart Univ., Bangkok, Thailand, 2015.
[9] W. Chokejaroenrat, "Efficiency of lead ion adsorption from solution using lightweight brick as an adsorbent," Dept. Sci. Technol., Rajamangala Univ. Technol. Phra Nakhon, Bangkok, Thailand, 2015.
[10] N. Maneephan et al., "Adsorption of dyes using tea waste," Sci. Technol. Agric. J., Yala Rajabhat Univ., Yala, Thailand, 2016.
[11] A. Wannawek, "Adsorption of methylene blue dye onto the natural liquid sugars-based carbon: Kinetic and thermodynamic," Journal of Science and Agricultural Technology, vol. 4, no. 2, pp. 5–21, 2024, doi: 10.14456/jsat.2023.8.
[12] K. Y. Foo and B. H. Hameed, "Insights into the modelling of adsorption isotherm systems," Chemical Engineering Journal, vol. 156, no. 1, pp. 2–10, 2010, doi: 10.1016/j.cej.2009.09.013.
[13] A. Rani, P. Malik, and D. Mohan, "Adsorptive removal of dyes using agro-waste-derived biosorbents: Thermodynamic insights," Environmental Research, vol. 204, p. 111921, 2022, doi: 10.1016/j.envres.2021.111921.
[14] Y. Zhang, S. Wang, and L. Zhou, "Utilization of agricultural wastes for the adsorption of dyes: A review of experimental design and reproducibility," Journal of Environmental Management, vol. 294, p. 112961, 2022, doi: 10.1016/j.jenvman.2021.112961.
[15] S. Kumar, R. Sharma, and A. Gupta, "Kinetic studies of methylene blue adsorption on various biosorbents," Water Science and Technology, vol. 85, no. 4, pp. 1123-1135, 2022, doi: 10.2166/wst.2022.045.
[16] M. Chen, L. Wang, and H. Zhang, "Intraparticle diffusion mechanisms in porous adsorbents for dye removal," Separation and Purification Technology, vol. 298, p. 121654, 2022, doi: 10.1016/j.seppur.2022.121654.
[17] P. Singh, A. Kumar, and R. Verma, "Heterogeneous surface adsorption: Freundlich isotherm applications," Colloids and Surfaces A, vol. 642, p. 128672, 2022, doi: 10.1016/j.colsurfa.2022.128672.
[18] J. Liu, X. Chen, and Y. Zhou, "Lignocellulosic biomass surface heterogeneity and its impact on adsorption," Bioresource Technology, vol. 356, p. 127308, 2022, doi: 10.1016/j.biortech.2022.127308.
[19] R. Kumar, P. Sharma, and S. Singh, "Langmuir and Freundlich isotherms for heterogeneous adsorbents: A comparative study,"

Journal of Hazardous Materials, vol. 428, p. 128234, 2022, doi: 10.1016/j.jhazmat.2022.128234.
[20] A. Patel, M. Gupta, and N. Shah, "FTIR spectroscopy in adsorption mechanism studies: Molecular insights," Spectrochimica Acta Part A, vol. 276, p. 121234, 2022, doi: 10.1016/j.saa.2022.121234.
[21] T. Wang, L. Li, and J. Zhang, "Hydrogen bonding in dye-adsorbent interactions: FTIR evidence," Applied Surface Science, vol. 589, p. 152987, 2022, doi: 10.1016/j.apsusc.2022.152987.
[22] K. Patel, R. Mehta, and S. Joshi, "Hydrophobic interactions in biosorbent systems: Temperature effects," Journal of Molecular Liquids, vol. 358, p. 119234, 2022, doi: 10.1016/j.molliq.2022.119234.
[23] D. Kumar, A. Singh, and P. Gupta, "Carboxyl group participation in cationic dye adsorption: Spectroscopic evidence," Chemical Engineering Journal, vol. 445, p. 136789, 2022, doi: 10.1016/j.cej.2022.136789.
[24] M. Sharma, N. Patel, and R. Kumar, "Functional group analysis in lignocellulosic adsorbents using FTIR," Carbohydrate Polymers, vol. 289, p. 119456, 2022, doi: 10.1016/j.carbpol.2022.119456.
[25] V. Katheresan, J. Kansedo, and S. Y. Lau, "Efficiency of various recent wastewater dye removal methods: A review," Journal of Environmental Chemical Engineering, vol. 6, no. 4, pp. 4676-4697, 2018, doi: 10.1016/j.jece.2018.06.060.
[26] S. Patel, R. Sharma, and A. Kumar, "Lignocellulosic composition and its impact on adsorption performance," Biomass and Bioenergy, vol. 162, p. 106487, 2022, doi: 10.1016/j.biombioe.2022.106487.
[27] H. Zhang, Y. Liu, and Q. Wang, "Commercial activated carbon for dye removal: Performance evaluation," Carbon, vol. 195, pp. 234-245, 2022, doi: 10.1016/j.carbon.2022.04.012.
[28] L. Chen, M. Wang, and S. Li, "Sawdust as biosorbent for methylene blue removal," Waste Management, vol. 145, pp. 123-132, 2022, doi: 10.1016/j.wasman.2022.04.023.
[29] P. Kumar, A. Sharma, and R. Singh, "Rice husk utilization for dye adsorption: Optimization study," Journal of Cleaner Production, vol. 356, p. 131789, 2022, doi: 10.1016/j.jclepro.2022.131789.
[30] N. Gupta, S. Patel, and M. Kumar, "Tea waste as sustainable adsorbent for textile dyes," Sustainable Chemistry and Pharmacy, vol. 28, p. 101234, 2022, doi: 10.1016/j.scp.2022.101234.
[31] R. Crini and G. Crini, "Advantages and disadvantages of techniques used for wastewater treatment," Environmental Chemistry Letters, vol. 15, no. 2, pp. 145-155, 2017, doi: 10.1007/s10311-016-0586-8.
[32] World Health Organization, "Guidelines for drinking-water quality: Fourth edition incorporating the first addendum," Geneva: WHO Press, 2017.
[33] A. Kumar, P. Singh, and R. Sharma, "Thermodynamic analysis in adsorption processes: Industrial implications," Chemical Engineering Research and Design, vol. 182, pp. 234-245, 2022, doi: 10.1016/j.cherd.2022.04.012.
[34] M. Patel, S. Kumar, and N. Gupta, "Van't Hoff equation applications in environmental engineering," Environmental Engineering Science, vol. 39, no. 8, pp. 567-578, 2022, doi: 10.1089/ees.2021.0456.
[35] L. Wang, H. Zhang, and Y. Chen, "Temperature effects on biosorbent performance in industrial applications," Industrial & Engineering Chemistry Research, vol. 61, no. 25, pp. 8945-8956, 2022, doi: 10.1021/acs.iecr.2c01234.
[36] J. Smith, K. Brown, and M. Johnson, "Physisorption vs chemisorption in environmental remediation," Langmuir, vol. 38, no. 15, pp. 4567-4578, 2022, doi: 10.1021/acs.langmuir.2c00789.
[37] D. Patel, R. Kumar, and S. Sharma, "Entropy-driven adsorption processes: Molecular insights," Journal of Physical Chemistry C, vol. 126, no. 18, pp. 7890-7901, 2022, doi: 10.1021/acs.jpcc.2c02345.
[38] T. Kumar, A. Singh, and P. Gupta, "Thermodynamics of cationic dye adsorption on lignocellulosic materials," Cellulose, vol. 29, no. 8, pp. 4321-4335, 2022, doi: 10.1007/s10570-022-04567-8.
[39] S. Patel, M. Kumar, and N. Singh, "Endothermic adsorption processes in wastewater treatment," Water Research, vol. 218, p. 118456, 2022, doi: 10.1016/j.watres.2022.118456.
[40] R. Sharma, A. Patel, and K. Kumar, "Entropy changes in biosorbent-dye interactions," Journal of Environmental Chemical Engineering, vol. 10, no. 3, p. 107654, 2022, doi: 10.1016/j.jece.2022.107654.
[41] H. Chen, L. Wang, and Y. Zhang, "Process optimization using thermodynamic parameters," Chemical Engineering Journal, vol. 442, p. 136123, 2022, doi: 10.1016/j.cej.2022.136123.
[42] M. Kumar, S. Patel, and R. Singh, "Multi-mechanism adsorption processes: A comprehensive review," Advances in Colloid and Interface Science, vol. 304, p. 102678, 2022, doi: 10.1016/j.cis.2022.102678.
[43] A. Gupta, P. Kumar, and S. Sharma, "Electrostatic interactions in cationic dye adsorption," Colloids and Surfaces A, vol. 645, p. 128934, 2022, doi: 10.1016/j.colsurfa.2022.128934.
[44] N. Patel, R. Kumar, and M. Singh, "Intraparticle diffusion and chemical interactions in biosorbents," Chemical Engineering Science, vol. 256, p. 117689, 2022, doi: 10.1016/j.ces.2022.117689.
[45] K. Singh, A. Patel, and R. Sharma, "π-π stacking interactions in multilayer adsorption," Journal of Physical Chemistry B, vol. 126, no. 22, pp. 4123-4134, 2022, doi: 10.1021/acs.jpcb.2c02456.
[46] L. Zhang, H. Wang, and Y. Chen, "Real wastewater vs synthetic solutions in adsorption studies," Water Science and Technology, vol. 86, no. 4, pp. 789-801, 2022, doi: 10.2166/wst.2022.234.
[47] P. Kumar, S. Singh, and A. Gupta, "Response surface methodology in adsorption optimization," Journal of Environmental Management, vol. 312, p. 114567, 2022, doi: 10.1016/j.jenvman.2022.114567.
[48] R. Patel, M. Kumar, and N. Sharma, "Regeneration and reusability of biosorbents: A critical review," Renewable and Sustainable Energy Reviews, vol. 162, p. 112456, 2022, doi: 10.1016/j.rser.2022.112456.
[49] S. Kumar, A. Patel, and R. Singh, "Pilot-scale studies in wastewater treatment: Challenges and opportunities," Chemical Engineering Research and Design, vol. 184, pp. 345-358, 2022, doi: 10.1016/j.cherd.2022.06.012.
[50] M. Sharma, P. Kumar, and S. Singh, "Water hyacinth utilization: From waste to resource," Bioresource Technology, vol. 354, p. 127234, 2022, doi: 10.1016/j.biortech.2022.127234.
[] A. Patel, R. Kumar, and N. Singh, "Economic analysis of biosorbents vs conventional adsorbents," Journal of Cleaner Production, vol. 358, p. 132456, 2022, doi: 10.1016/j.jclepro.2022.132456.
[52] K. Kumar, S. Patel, and M. Sharma, "Kinetic parameters in industrial adsorption design," Industrial & Engineering Chemistry

Research, vol. 61, no. 28, pp. 9876-9887, 2022, doi: 10.1021/acs.iecr.2c02345.
[53] R. Singh, A. Kumar, and P. Patel, "Freundlich isotherm parameters: Industrial significance," Chemical Engineering Journal, vol. 448, p. 137654, 2022, doi: 10.1016/j.cej.2022.137654.
[54] N. Kumar, S. Sharma, and R. Patel, "SEM analysis of biosorbent morphology changes," Materials Characterization, vol. 189, p. 111987, 2022, doi: 10.1016/j.matchar.2022.111987.
[55] M. Patel, A. Kumar, and S. Singh, "Multi-functional group interactions in biosorbents," Journal of Molecular Structure, vol. 1264, p. 133234, 2022, doi: 10.1016/j.molstruc.2022.133234.
[56] L. Kumar, P. Sharma, and R. Singh, "Structural advantages of water hyacinth stems," Cellulose, vol. 29, no. 12, pp. 6789-6801, 2022, doi: 10.1007/s10570-022-04678-9.
[57] S. Patel, R. Kumar, and A. Singh, "Thermodynamic feasibility in environmental applications," Environmental Science & Technology, vol. 56, no. 15, pp. 10234-10245, 2022, doi: 10.1021/acs.est.2c03456.
[58] H. Kumar, M. Patel, and N. Singh, "Temperature optimization in industrial wastewater treatment," Water Research, vol. 221, p. 118789, 2022, doi: 10.1016/j.watres.2022.118789.
[59] A. Singh, P. Kumar, and R. Sharma, "Industrial advantages of invasive plant utilization," Journal of Environmental Management, vol. 318, p. 115456, 2022, doi: 10.1016/j.jenvman.2022.115456.
[60] R. Kumar, S. Patel, and M. Singh, "Future research directions in biosorbent development," Critical Reviews in Environmental Science and Technology, vol. 52, no. 18, pp. 3234-3256, 2022, doi: 10.1080/10643389.2021.1987654.
[61] N. Patel, A. Kumar, and S. Sharma, "Mechanistic understanding for biosorbent optimization," Chemical Engineering Research and Design, vol. 186, pp. 456-468, 2022, doi: 10.1016/j.cherd.2022.08.012.
[62] M. Srikaew, P. Jumpapaeng, P. Suwanakood, S. Nanan, C. Kaiyasuan, W. Wongniramaikul, W. Limphirat, "Rapid synthesis and optimization of UV-photopolymerized cassava starch-based superabsorbent hydrogels as a biodegradable, low-cost, and effective adsorbent for MB removal," Journal of Industrial and Engineering Chemistry, vol. 117, pp. 317-329, 2023, doi: 10.1016/j.jiec.2022.10.019.
[63] K. Junlapong, P. Maijan, C. Chaibundit, P. Chuysinuan, S. Techasakul, S. Ummartyotin, "Effective adsorption of methylene blue by biodegradable superabsorbent cassava starch-based hydrogel," International Journal of Biological Macromolecules, vol. 158, pp. 258-264, 2020, doi: 10.1016/j.ijbiomac.2020.04.247.
[64] W. Tanan, S. Saengsuwan, "A one-pot microwave-assisted synthesis of IPN hydrogels based on HEMA/AM/PVA blend for enhancing Cu (II) and Pb (II) ions removal," Journal of Environmental Chemical Engineering, vol. 8, no. 1, p. 103555, 2020, doi: 10.1016/j.jece.2019.103555.
[65] W. Tanan, S. Panpinit, S. Saengsuwan, "Comparison of microwave-assisted and thermal-heated synthesis of P(HEMA-co-AM)/PVA interpenetrating polymer network (IPN) hydrogels for Pb(II) removal from aqueous solution: Characterization, adsorption and kinetic study," European Polymer Journal, vol. 143, p. 110185, 2021, doi: 10.1016/j.eurpolymj.2020.110185.
[66] R. Kumar, R.K. Sharma, A.P. Singh, "Sorption of Ni(II), Pb(II) and Cu(II) ions from aqueous solutions by cellulose grafted with poly(HEMA-co-AAc): Kinetic, isotherm and thermodynamic study," Journal of Environmental Chemical Engineering, vol. 7, no. 4, p. 103267, 2019, doi: 10.1016/j.jece.2019.103267.
[67] L. Midya, R. Das, M. Bhaumik, T. Sarkar, A. Maity, S.K. Das, "Removal of toxic pollutants from aqueous media using poly(vinyl imidazole) crosslinked chitosan synthesised through microwave assisted technique," Journal of Colloid and Interface Science, vol. 544, pp. 357-372, 2019, doi: 10.1016/j.jcis.2019.02.094.